REGULAR ARTICLE

blood advances

RNA-regulatory exosome complex suppresses an apoptotic program to confer erythroid progenitor cell survival in vivo

Isabela Fraga de Andrade,[1] Kirby D. Johnson,[1] Charu Mehta,[1] Colin N. Dewey,[2] Uttiya Basu,[3] and Emery H. Bresnick[1]

[1]University of Wisconsin-Madison Blood Cancer Research Program, Department of Cell and Regenerative Biology, Wisconsin Institutes for Medical Research, University of Wisconsin School of Medicine and Public Health, Madison, WI; [2]Department of Biostatistics and Medical Informatics, University of Wisconsin, Madison, WI; and [3]Department of Microbiology and Immunology, Vagelos College of Physicians and Surgeons, Columbia University, New York, NY

Key Points

- *Exosc3* expression in the hematopoietic system is essential for mouse embryogenesis.
- Exosc3 confers erythroid progenitor survival and activity in vivo by suppressing an apoptotic gene expression program.

The RNA-regulatory exosome complex (EC) posttranscriptionally and cotranscriptionally processes and degrades RNAs in a context-dependent manner. Although the EC functions in diverse cell types, its contributions to stem and progenitor cell development are not well understood. Previously, we demonstrated that the transcriptional regulator of erythrocyte development, GATA1, represses EC subunit genes, and the EC maintains erythroid progenitors in vitro. To determine if this mechanism operates in vivo, we used the hematopoietic-specific Vav1-Cre and "conditional by inversion" mouse system to ablate *Exosc3*, encoding an EC structural subunit. Although *Exosc3*$^{C/C}$ Cre^{+} embryos developed normally until embryonic day 14.5, *Exosc3* ablation was embryonic lethal and severely reduced erythromyeloid progenitor activity. RNA sequencing analysis of *Exosc3*-ablated burst-forming unit-erythroid revealed elevated transcripts encoding multiple proapoptotic factors, and the mutant erythroid progenitors exhibited increased apoptosis. We propose that the EC controls an ensemble of apoptosis-regulatory RNAs, thereby promoting erythroid progenitor survival and developmental erythropoiesis in vivo.

Introduction

The evolutionarily conserved RNA-regulatory exosome complex (EC) functions to synthesize, process, and degrade diverse coding and noncoding RNA transcripts. EC components were identified as 3' to 5' exoribonucleases required for 5.8 Svedberg units (S) ribosomal RNA (rRNA) processing in yeast.[1,2] Loss-of-function studies revealed an EC role in processing diverse RNAs and regulating important biological processes.[3-6] In mammalian cells, the EC interacts with other RNA-processing components to target coding and noncoding transcripts in a context-specific manner.[7,8] Although EC molecular attributes have been rigorously analyzed, it is unclear how it controls biological processes in cells and tissues of complex organisms.

The extensive transcriptomic remodeling required for stem and progenitor cell differentiation involves transcriptional and posttranscriptional mechanisms. For erythropoiesis, in which hematopoietic stem cells (HSCs) generate committed progenitors, GATA1[9,10] regulates a large gene cohort required for erythroid maturation and erythrocyte function.[11-15] GATA1 represses genes encoding EC subunits at an early stage of erythroblast maturation in mouse and human cells.[6,16,17] Downregulating the structural subunits, Exosc8 and Exosc9, using short hairpin RNAs disrupts EC integrity in primary erythroid

Submitted 1 July 2022; accepted 31 August 2022; prepublished online on *Blood Advances* First Edition 26 September 2022. https://doi.org/10.1182/bloodadvances.2022008481.

The sequencing data reported in this article have been deposited in the Gene Expression Omnibus database (accession number GSE203607).

Data are available on request from the corresponding author, Emery H. Bresnick (ehbresni@wisc.edu).

The full-text version of this article contains a data supplement.

© 2023 by The American Society of Hematology. Licensed under Creative Commons Attribution-NonCommercial-NoDerivatives 4.0 International (CC BY-NC-ND 4.0), permitting only noncommercial, nonderivative use with attribution. All other rights reserved.

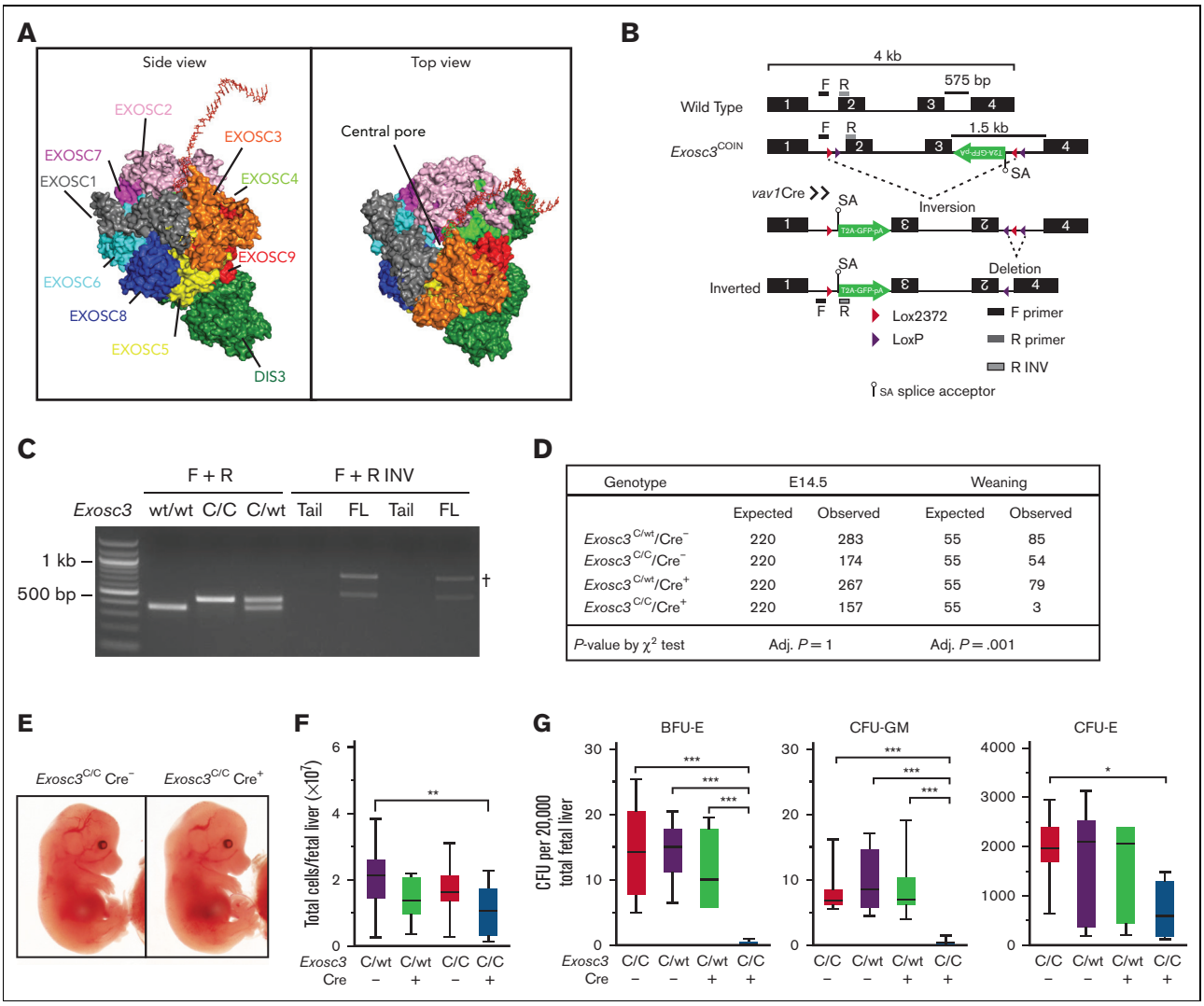

Figure 1. *Exosc3* expression in the hematopoietic system is required for hematopoietic progenitor activity and embryogenesis. (A) Crystal structure and model of the human EC bound by a synthetic 16 base pair RNA molecule.[19] (B) *Exosc3* conditional ablation strategy with Cre recombinase expression controlled by the hematopoietic promoter *Vav1*. Cre recognizes the loxP and lox2372 sites within *Exosc3* and promotes inversion, followed by deletion. A GFP cassette is activated after inversion and serves as a recombination marker. Forward (F) and reverse (R) primer sets were used to distinguish wild-type (WT) from conditional by inversion (COIN = C) allele. F and R-inverted (R INV) primer set was used to detect the inverted C allele in hematopoietic tissue. Primer alignment is depicted as black and gray boxes. (C) PCR-based genotyping of WT (expected size of 300 base pair) and *Exosc3* COIN allele (expected size of 400 base pair) and amplification of inverted allele (expected size of 500 base pair) specific to hematopoietic tissue. gDNA was obtained from tail clip of $Exosc3^{WT/WT}$ Cre^{-}, $Exosc3^{C/C}$, and $Exosc3^{C/WT}$ mice for the first 3 lanes. gDNA was obtained from tail clip and fetal liver (FL) of $Exosc3^{C/C}$ Cre^{+} embryos (2 biological reps) for the 4 lanes below F + R INV. Tail gDNA was used as a negative control for the F + R INV PCR reaction. (D) Embryo genotypes at the indicated developmental stages. The χ-square *P* values refer to $Exosc3^{C/C}$ Cre^{+} in comparison with control $Exosc3^{C/C}$ Cre^{-}. (E) Representative E14.5 $Exosc3^{C/C}$ Cre^{-} and $Exosc3^{C/C}$ Cre^{+} embryos. (F) Fetal liver cell enumeration (13 independent experiments: $Exosc3^{C/C}$ $Cre^{-} = 14$, $Exosc3^{C/WT}$ $Cre^{-} = 33$, $Exosc3^{C/WT}$ $Cre^{+} = 28$, and $Exosc3^{C/C}$ $Cre^{+} = 14$). (G) E14.5 fetal liver cells were plated in a CFU media at 20 000 cells per mL (5 independent experiments: $Exosc3^{C/wt}$ $Cre^{-} = 13$, $Exosc3^{C/wt}$ $Cre^{+} = 7$, $Exosc3^{C/C}$ $Cre^{-} = 10$ and $Exosc3^{C/C}$ $Cre^{+} = 10$). Quantitative data are presented as box and whisker plots, with bounds from the 25th to 75th percentiles, the median line, and whiskers ranging from minimum to maximum values. $^{*}P < .05$, $^{**}P < .01$, and $^{***}P < .001$, by Tukey multiple comparisons test. † indicates nonspecific band; adj, adjusted.

precursors and depletes the burst-forming unit-erythroid (BFU-E) progenitor.[16,17] In immature erythroblasts, the EC promotes c-kit receptor tyrosine kinase expression (KIT) and suppresses expression of the erythropoietin (Epo) receptor that mediates prodifferentiation signaling.[16,17] Downregulation of the EC catalytic subunit, DIS3, using short hairpin RNAs in primary erythroid precursors triggers apoptosis, which correlates with reduced *Kit* expression and elevated DNA damage.[6]

We developed a hematopoietic-specific in vivo knockout strategy to ablate *Exosc3*, encoding a structural component with conserved S1 and K homology RNA-binding domains.[18] Based on 2 pairs of lox sites in introns 1 and 3,[4] *Vav1*-regulated Cre disrupted *Exosc3* in hematopoietic cells, which impaired fetal hematopoiesis and erythromyeloid progenitor activity. Exosc3-deficient progenitors failed to form BFU-Es, expressed reduced cell-surface KIT levels, and were apoptotic. *Exosc3* ablation upregulated transcripts encoding BCL-2

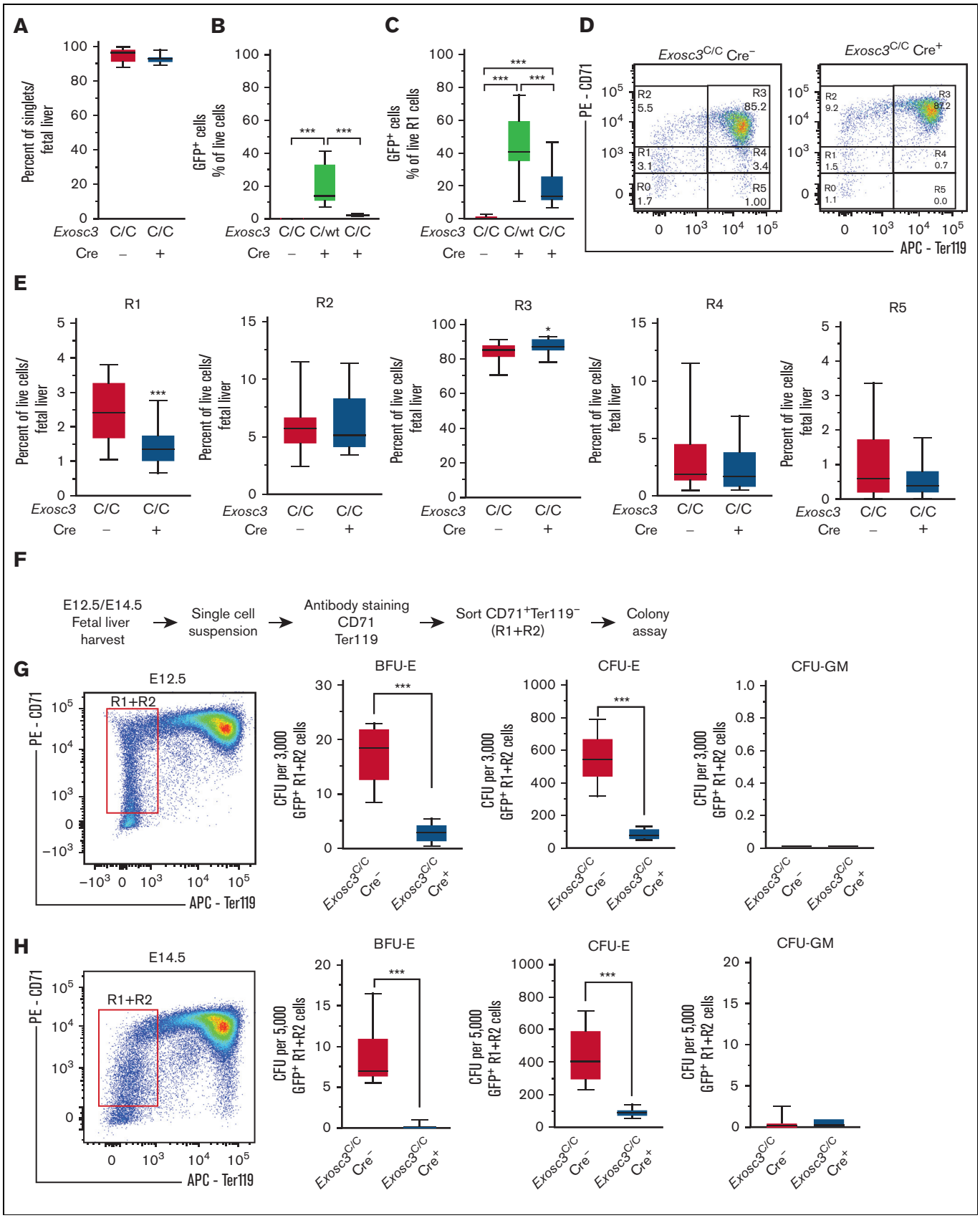
A
Percent of singlets/ fetal liver
Exosc3 C/C C/C
Cre – +
B
GFP+ cells % of live cells
Exosc3 C/C C/wt C/C
Cre – + +
C
GFP+ cells % of live R1 cells
Exosc3 C/C C/wt C/C
Cre – + +
D
Exosc3C/C Cre–
Exosc3C/C Cre+
PE - CD71
APC - Ter119
R0 1.7
R1 3.1
R2 5.5
R3 85.2
R4 3.4
R5 1.00
R0 1.1
R1 1.5
R2 9.2
R3 87.2
R4 0.7
R5 0.0
E
R1
R2
R3
R4
R5
Percent of live cells/ fetal liver
Exosc3 C/C C/C
Cre – +
F
E12.5/E14.5 Fetal liver harvest
Single cell suspension
Antibody staining CD71 Ter119
Sort CD71+Ter119– (R1+R2)
Colony assay
G
E12.5
R1+R2
PE - CD71
APC - Ter119
BFU-E
CFU-E
CFU-GM
CFU per 3,000 GFP+ R1+R2 cells
Exosc3C/C Cre–
Exosc3C/C Cre+
H
E14.5
R1+R2
PE - CD71
APC - Ter119
BFU-E
CFU-E
CFU-GM
CFU per 5,000 GFP+ R1+R2 cells
Exosc3C/C Cre–
Exosc3C/C Cre+

Figure 2.

family proapoptotic factors, Fas death receptor, and p53 pathway components. Thus, EC function is vital for erythroid progenitors before GATA1-mediated erythroid differentiation in vivo.

Methods

Mice

Exosc3-floxed mice were described previously.[4] Vav1-Cre mice were provided by Jing Zhang (University of Wisconsin-Madison). Mouse experiments were performed with the ethical approval of Association for the Assessment and Accreditation of Laboratory Animal Care International at University of Wisconsin-Madison.

Colony-forming unit assays

For fetal liver colony–forming unit assays, embryonic day 14.5 (E14.5) fetal liver cells were dissociated and plated in duplicate in methylcellulose (MethoCult M3434, StemCell Technologies) at the indicated concentrations. Colony-forming unit-erythroid (CFU-E) were scored on day 3, and colony-forming unit–granulocyte macrophage (CFU-GM) and BFU-E were scored on day 8. Megakaryocyte erythrocyte progenitor (MEP)–derived colonies were scored on day 5.

Locus disruption analysis

Sorted green fluorescent protein$^+$ (GFP$^+$) and GFP$^-$ erythroid progenitors (CD71$^{\text{low-intermediate}}$ Ter119$^-$) (30 000-50 000) were sorted and processed as described in supplemental Methods. Real-time polymerase chain reaction (PCR) was conducted with SYBR Green master mix using a Viia7 instrument (Applied Biosystems) and primers flanking the *loxP* site. Relative values were calculated from a standard curve of serial dilutions of genomic DNA (gDNA) samples and normalized to the *Polr2a* promoter.

Gene expression analysis

Total RNA was purified from cells using TRIzol (Invitrogen). Complementary DNA was synthesized by Moloney murine leukemia virus reverse transcription (Thermo Fisher Scientific). Real-time PCR was conducted with SYBR Green master mix (Thermo Fisher Scientific). Control reactions lacking Moloney murine leukemia virus reverse transcription yielded little to no signal. Relative expression was calculated from a standard curve of complementary DNA serial dilutions, and values were normalized to 18S RNA expression. Primer sequences are shown in supplemental Table 3.

Flow cytometry

Sample preparation details are provided in supplemental Methods. Data were acquired on an Attune NxT Flow Cytometer (Thermo Fisher Scientific) or collected on a BD FACSAria II Cell Sorter (BD Biosciences). The data were analyzed using FlowJo version 10.1 software (TreeStar). 4′,6-diamidino-2-phenylindole (DAPI) (422801, BioLegend) was used for live/dead discrimination in all assays.

Apoptosis analysis

Lineage-depleted progenitors were stained with Lin$^+$, CD71, CD24, and KIT. Cells were stained with DRAQ7 and Annexin V pacific blue (ThermoFisher Scientific, A35122) and analyzed on an Attune NxT Flow Cytometer.

Statistics

For quantitative analysis of cell numbers, DNA, messenger RNA (mRNA), and flow cytometric data, when comparing >2 experimental groups, significance was assessed using Tukey multiple comparisons test. When comparing 2 experimental conditions, significance was assessed using 2-tailed unpaired Student *t* test, unless otherwise indicated. $P < .05$ was considered significant. GraphPad Prism 6 (GraphPad Software) was used for data analysis and graph generation.

RNA-seq

E14.5 fetal livers (n = 6, 2 from each of 3 litters) were processed, and GFP$^+$ and GFP$^-$ Lin$^-$KIT$^+$CD24/71$^{10\%\text{low}}$ BFU-Es were sorted as described in supplemental Methods. Cells were analyzed for CFU assay (2600 cells per mL), and RNA was used for RNA sequencing (RNA-seq). RNA libraries were prepared using the SMARTer Stranded Total RNA-Seq Kit version 2 (Takara) Pico Library Prep with random hexamers for the reverse transcription reaction. RNA-seq data were generated with an NovaSeq 6000 System sequencer (Illumina) as 151 base pair paired-end reads. Sample processing and analysis details are presented in the supplemental Data.

Results

Expression of EC subunit Exosc3 in the hematopoietic system is required for embryogenesis

Because GATA1 represses EC subunit genes and in vitro studies implicated EC in erythroid progenitor survival and differentiation,[16,17] we generated a hematopoietic-specific knock out of *Exosc3* to test whether these results can be extrapolated to erythroblasts in an in vivo microenvironment. Exosc3 associates with Exosc1 and Exosc2 to form an RNA-binding cap to the EC barrel structure, which directs transcripts through the central pore for processing/degradation (Figure 1A). Mice containing a COIN *Exosc3* allele were crossed to *Vav1*-Cre mice to ablate *Exosc3* in hematopoietic cells.[4] Cre-mediated recombination of lox sites

Figure 2. *Exosc3* expression in the hematopoietic system confers erythroid progenitor activity in an erythroid cell–intrinsic manner. (A) *Exosc3* ablation did not affect cellular viability, assessed by DAPI staining. (B) GFP$^+$ percentage of live fetal liver cells. Significance by Tukey multiple comparisons test. (C) GFP$^+$ percentage from live R1 cells parent gate. Significance by Tukey multiple comparisons test. (D) Representative flow cytometric plots depicting erythroid maturation based on CD71 and Ter119 expression in *Exosc3*$^{C/C}$ Cre$^-$ and *Exosc3*$^{C/C}$ Cre$^+$ E14.5 embryos (13 independent experiments: *Exosc3*$^{C/C}$ Cre$^-$ = 21 and *Exosc3*$^{C/C}$ Cre$^+$ = 17). (E) Quantification of R1 to R4 populations from E14.5 fetal livers. (F) Experimental scheme for assessing CFU activity of *Exosc3*$^{C/C}$ Cre$^-$ and *Exosc3*$^{C/C}$ Cre$^+$ of sorted GFP$^+$ R1 + R2 from E12.5 or E14.5 fetal livers. Colonies were quantified after 3 days (CFU-E) or 8 days (BFU-E and CFU-GM) in methylcellulose. (G) CFU activity of *Exosc3*$^{C/C}$ Cre$^-$ and *Exosc3*$^{C/C}$ Cre$^+$ 3000 sorted GFP$^+$ R1 + R2 cells from E12.5 fetal livers (7 independent experiments: *Exosc3*$^{C/C}$ Cre$^-$ = 7 and *Exosc3*$^{C/C}$ Cre$^+$ = 6). (H) CFU activity of *Exosc3*$^{C/C}$ Cre$^-$ and *Exosc3*$^{C/C}$ Cre$^+$ with 5000 sorted GFP$^+$ R1 + R2 from E14.5 fetal livers (7 independent experiments: *Exosc3*$^{C/C}$ Cre$^-$ = 9 and *Exosc3*$^{C/C}$ Cre$^+$ = 6). Quantitative data are presented as box and whisker plots, with bounds from the 25th to 75th percentiles, the median line, and whiskers ranging from minimum to maximum values. *$P < .05$, **$P < .01$, and ***$P < .001$, by unpaired *t* test. APC, allophycocyanin.

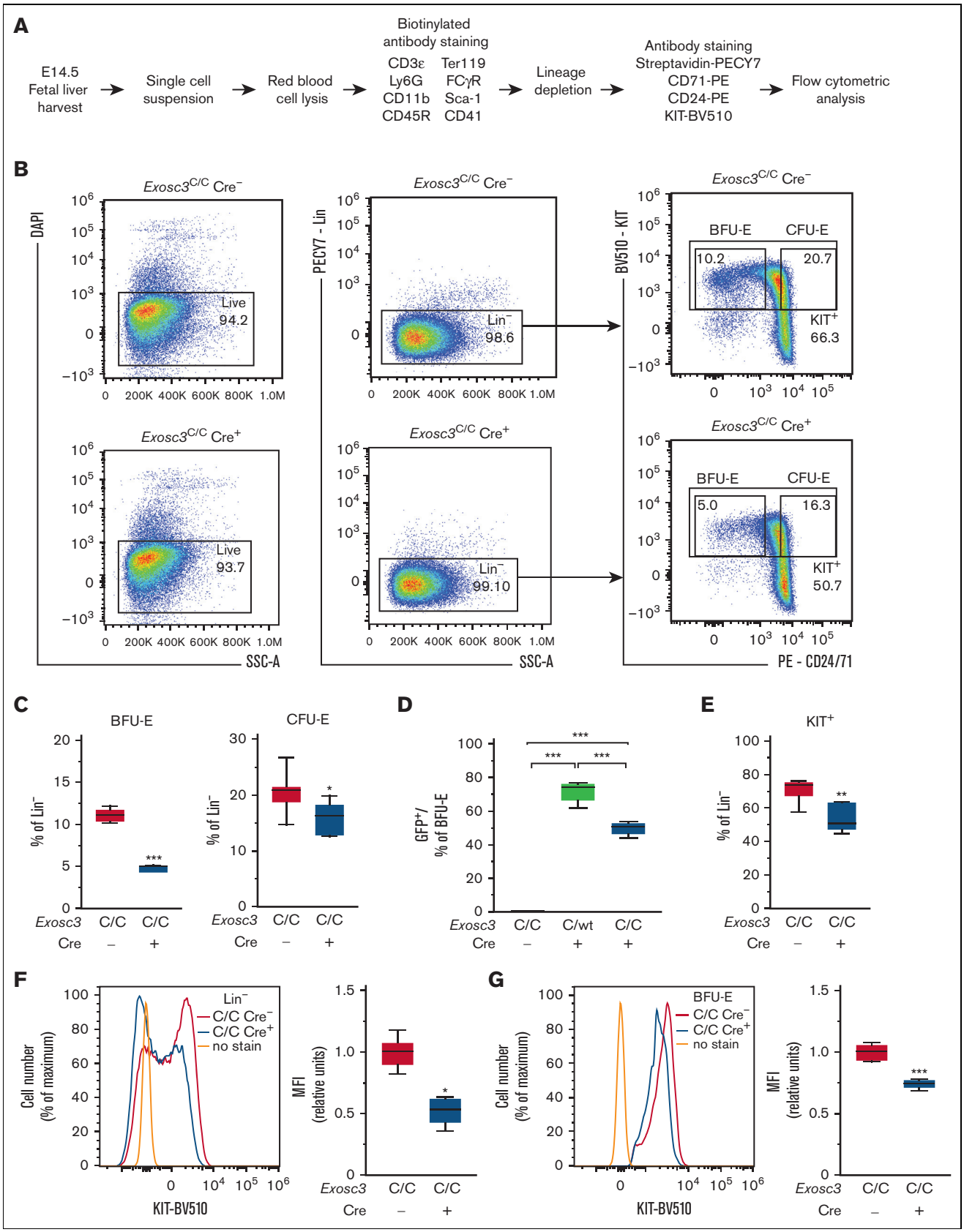
A
E14.5 Fetal liver harvest
Single cell suspension
Red blood cell lysis
Biotinylated antibody staining
CD3ε Ter119
Ly6G FCγR
CD11b Sca-1
CD45R CD41
Lineage depletion
Antibody staining Streptavidin-PECY7
CD71-PE
CD24-PE
KIT-BV510
Flow cytometric analysis
B
Exosc3C/C Cre−
Exosc3C/C Cre+
DAPI
SSC-A
Live 94.2
Live 93.7
PECY7 - Lin
Lin− 98.6
Lin− 99.10
BV510 - KIT
PE - CD24/71
BFU-E
CFU-E
10.2
20.7
KIT+ 66.3
5.0
16.3
KIT+ 50.7
C
BFU-E
CFU-E
% of Lin−
Exosc3 C/C C/C
Cre − +
D
GFP+/ % of BFU-E
Exosc3 C/C C/wt C/C
Cre − + +
E
KIT+
% of Lin−
Exosc3 C/C C/C
Cre − +
F
Lin−
C/C Cre−
C/C Cre+
no stain
Cell number (% of maximum)
KIT-BV510
MFI (relative units)
Exosc3 C/C C/C
Cre − +
G
BFU-E
C/C Cre−
C/C Cre+
no stain
Cell number (% of maximum)
KIT-BV510
MFI (relative units)
Exosc3 C/C C/C
Cre − +

Figure 3.

within introns 1 and 3 promotes inversion between the lox2372 sequences and deletion between the loxP sites, thus, corrupting the *Exosc3* open reading frame (Figure 1B). The inversion induces *Exosc3* promoter–dependent GFP expression as a metric of locus disruption. PCR analysis was used to distinguish the WT allele and the COIN noninverted allele and to detect the COIN-inverted alleles, which were specific to hematopoietic tissue (Figure 1C). The *Vav1* promoter is activated at approximately E9.5-E10.5 when HSCs emerge in the aorta-gonad-mesonephros region of the mouse embryo and is active in all hematopoietic lineages.[20-24]

The intercross between *Exosc3*$^{C/C}$ Cre^{-} and *Exosc3*$^{C/WT}$ Cre^{+} mice yielded only 3 *Exosc3*$^{C/C}$ Cre^{+} animals at weaning of 221 total (1.3%), far below the expected Mendelian ratio (25%), indicating that *Exosc3* expression in the hematopoietic system is required for embryogenesis (Figure 1D). The 3 *Exosc3*$^{C/C}$ Cre^{+} mice had normal blood count and did not show defective hematopoiesis in the steady state (data not shown). Analyses at E12.5 and E14.5 revealed that *Exosc3*$^{C/C}$ Cre^{+} embryos lacked obvious developmental abnormalities and signs of anemia or hemorrhage. Fetal liver cell numbers were slightly decreased in *Exosc3*$^{C/C}$ Cre^{+} embryos in comparison with *Exosc3*$^{C/WT}$ Cre^{-} embryos ($P = .002$) (Figure 1E-F; supplemental Figure 1A-B). To test if *Exosc3* ablation in the hematopoietic system affects hematopoietic progenitor activity, E14.5 fetal liver cells (20 000/mL) were analyzed in a CFU assay. *Exosc3*$^{C/C}$ Cre^{+} cells generated reduced BFU-E (mean ± standard error of the mean [SEM], 0.25 ± 0.13 vs 14.45 ± 2.23; $P < .0001$) and CFU-GM (mean ± SEM, 0.25 ± 0.15 vs 7.9 ± 1.0; $P < .0001$) in comparison with *Exosc3*$^{C/C}$ Cre^{-} cells. CFU-Es were reduced significantly with *Exosc3*$^{C/C}$ Cre^{+} cells in comparison with *Exosc3*$^{C/C}$ Cre^{-} cells (mean ± SEM, 713.5 ± 189.4 vs 1960 ± 202.7; $P = .01$) (Figure 1G). Thus, *Exosc3* expression in the hematopoietic system is required for erythroid and myeloid progenitor activity during fetal development.

To validate the *Exosc3* ablation, primers were designed to target a region flanking the loxP sites, which is corrupted by Cre recombinase–mediated inversion (supplemental Figure 1C). GFP^{+} erythroid cells (CD71^{+}Ter119^{-}) were fluorescence-activated cell sorting–sorted for gDNA and RNA isolation. *Exosc3*$^{C/C}$ Cre^{+} CD71^{+}Ter119^{-} GFP^{+} precursors showed a loss of 72% ($P < .0001$) of loxP site relative to control *Exosc3*$^{C/C}$ Cre^{-} cells at E12.5 (supplemental Figure 1D). The locus disruption in the GFP^{+} population reduces *Exosc3* mRNA by 60% and 50% at E12.5 and E14.5, respectively ($P = .0012$ and $P = .0327$, respectively) (supplemental Figure 1E-F). Sorted GFP^{-} erythroid precursors from *Exosc3*$^{C/C}$ Cre^{+} were analyzed as a control and had levels of unrecombined allele and *Exosc3* mRNA comparable to *Exosc3*$^{C/C}$ Cre^{-} cells.

The loss of BFU-E colonies might result from BFU-E cell depletion or defective progenitor activity. To test these possibilities, we used flow cytometry with erythroid cell–surface markers, CD71 and Ter119, to determine if *Exosc3* ablation affected immunophenotypic erythroid progenitors and to define the maturation stage of live DAPI^{-} erythroblasts in E14.5 fetal liver (Figure 2A). In *Exosc3*$^{C/C}$ Cre^{+} fetal liver, 2% of live cells expressed GFP, whereas in *Exosc3*$^{C/WT}$/Cre^{+} fetal liver, 20% of live cells expressed the inversion reporter (Figure 2B). Within the progenitor-enriched R1 subpopulation, 43% and 19% of cells expressed GFP in *Exosc3*$^{C/WT}$ Cre^{+} and *Exosc3*$^{C/C}$ Cre^{+} conditions, respectively (Figure 2C). Erythroid maturation (R1-R5) was assessed with CD71 and Ter119 (Figure 2D). The R1 subpopulation and precursors decreased 40%, from 2.5% to 1.5% ($P = .0003$), whereas early and late basophilic erythroblasts enriched in R3 increased 3.6%, from 84% to 87% ($P = .0285$), with *Exosc3*$^{C/C}$ Cre^{+} in comparison with *Exosc3*$^{C/C}$ Cre^{-} conditions (Figure 2E). Polychromatic and orthochromatic erythroblasts and reticulocytes enriched in R4 and R5, respectively, were comparable to control. Thus, although *Exosc3* ablation abrogated progenitor activity, immunophenotypic progenitors could still be detected at decreased levels.

Cell-intrinsic Exosc3 requirement in erythroid progenitor cells

To rigorously establish if the *Exosc3* requirement for erythroid progenitor activity reflects an erythroid cell–intrinsic mechanism, GFP^{+} CD71^{+}Ter119^{-} erythroid cells (R1 + R2) from E12.5 and E14.5 embryos were isolated by flow cytometry and plated in methylcellulose (3000/mL and 5000/mL, respectively) (Figure 2F). *Exosc3* ablation reduced BFU-E and CFU-E. At E12.5, BFU-E decreased 84% from 17.6 ± 2.0 to 2.91 ± 0.7 ($P < .0001$), and CFU-Es decreased 85%, from 550 ± 65.3 to 84 ± 15.7 ($P = .0001$) (Figure 2G). At E14.5, BFU-E decreased 92%, from 8.7 ± 1.2 to 0.17 ± 0.1 ($P < .0001$), and CFU-E decreased 79%, from 435 ± 55.3 to 91.5 ±11.3 ($P = .0003$) (Figure 2H). As expected, the sorted erythroid CD71^{+} progenitors did not yield nonerythroid CFU-GM colonies. These results indicate that *Exosc3*-ablated erythroid progenitors have a cell-intrinsic defect in erythroid colony generation, consistent with a model in which the EC is essential for erythroid progenitor activity before GATA1 repression during erythroid differentiation.

As Exosc3 expression is required for BFU-E activity, and its loss modestly decreased an erythroid progenitor–enriched immunophenotypic population, we used a more refined flow cytometric assay to detect BFU-E.[25] BFU-E were defined as the subset (10%) of KIT^{+} cells of lineage-depleted progenitors with the lowest expression of the early erythroid antigens CD24 and CD71, including CD24^{-}/CD71^{-} cells. CFU-E were defined as the subset (20%) of KIT^{+} cells with the highest CD24 and CD71 expression. Lineage-depleted (Lin^{-}) fetal liver hematopoietic progenitors were stained for KIT, CD24, and CD71 and analyzed by flow cytometry (Figure 3A-B). *Exosc3*$^{C/C}$ Cre^{+} fetal livers had 57.3% fewer Lin^{-}KIT^{+}CD24/71$^{10\%low}$ BFU-E (4.7%) in comparison with control

Figure 3. *Exosc3* ablation reduces immunophenotypic BFU-E and KIT cell-surface surface expression. (A) Experimental strategy. (B) Representative flow plots depicting erythroid maturation based on KIT, CD71, and CD24 expression to discriminate BFU-E (Lin^{-}KIT^{+}CD24/71$^{10\%low}$) and CFU-E (Lin^{-}KIT^{+}CD24/71$^{20\%high}$) populations in *Exosc3*$^{C/C}$ Cre^{-} and *Exosc3*$^{C/C}$ Cre^{+} E14.5 embryos. (C) Quantification of Lin^{-}KIT^{+}CD24/71$^{10\%low}$ BFU-E and Lin^{-}KIT^{+}CD24/71$^{20\%high}$ CFU-E (3 independent experiments: *Exosc3*$^{C/C}$ Cre^{-} = 8 and *Exosc3*$^{C/C}$ Cre^{+} = 5). (D) GFP percentage in BFU-E gate for *Exosc3*$^{C/C}$ Cre^{-}, *Exosc3*$^{C/WT}$ Cre^{+}, and *Exosc3*$^{C/C}$ Cre^{+} conditions. Significance by Tukey multiple comparisons test. (E) KIT^{+} cells within Lin^{-} progenitor population. (F) KIT cell-surface expression within Lin^{-} progenitors. (G) KIT cell-surface expression in Lin^{-}KIT^{+}CD24/71$^{10\%low}$ BFU-E population. Quantitative data are presented as box and whisker plots, with bounds from the 25th to 75th percentiles, the median line, and whiskers ranging from minimum to maximum values. *$P < .05$, **$P < .01$, and ***$P < .001$, by unpaired *t* test.

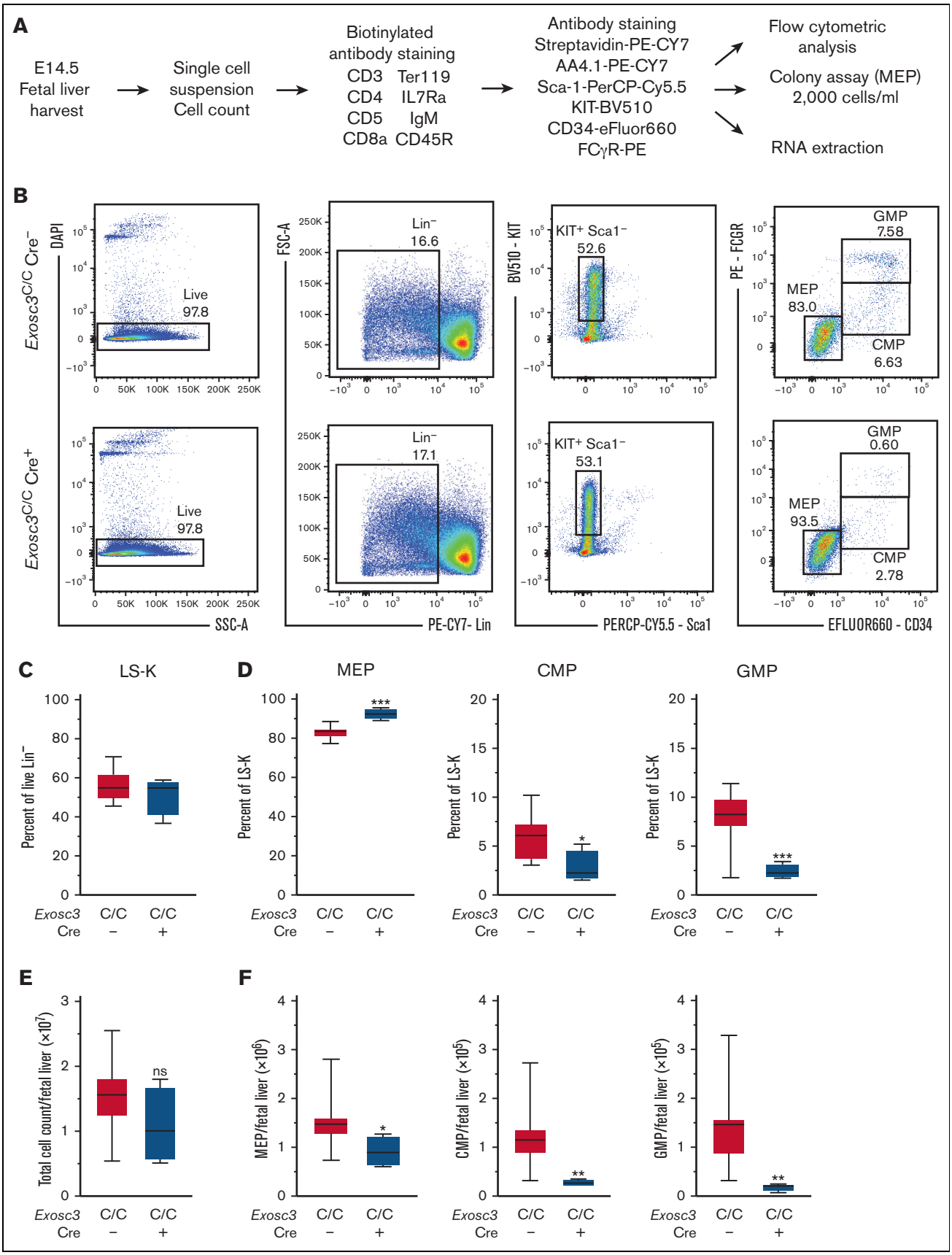
A
E14.5
Fetal liver
harvest
Single cell
suspension
Cell count
Biotinylated
antibody staining
CD3 Ter119
CD4 IL7Ra
CD5 IgM
CD8a CD45R
Antibody staining
Streptavidin-PE-CY7
AA4.1-PE-CY7
Sca-1-PerCP-Cy5.5
KIT-BV510
CD34-eFluor660
FCγR-PE
Flow cytometric
analysis
Colony assay (MEP)
2,000 cells/ml
RNA extraction
B
Exosc3C/C Cre−
Exosc3C/C Cre+
DAPI
Live
97.8
SSC-A
FSC-A
Lin−
16.6
Lin−
17.1
PE-CY7- Lin
BV510 - KIT
KIT+ Sca1−
52.6
KIT+ Sca1−
53.1
PERCP-CY5.5 - Sca1
PE - FCGR
EFLUOR660 - CD34
GMP
7.58
MEP
83.0
CMP
6.63
GMP
0.60
MEP
93.5
CMP
2.78
C
LS-K
Percent of live Lin−
D
MEP
CMP
GMP
Percent of LS-K
Exosc3 C/C C/C
Cre − +
E
Total cell count/fetal liver (×10^7)
ns
F
MEP/fetal liver (×10^6)
CMP/fetal liver (×10^5)
GMP/fetal liver (×10^5)

Figure 4.

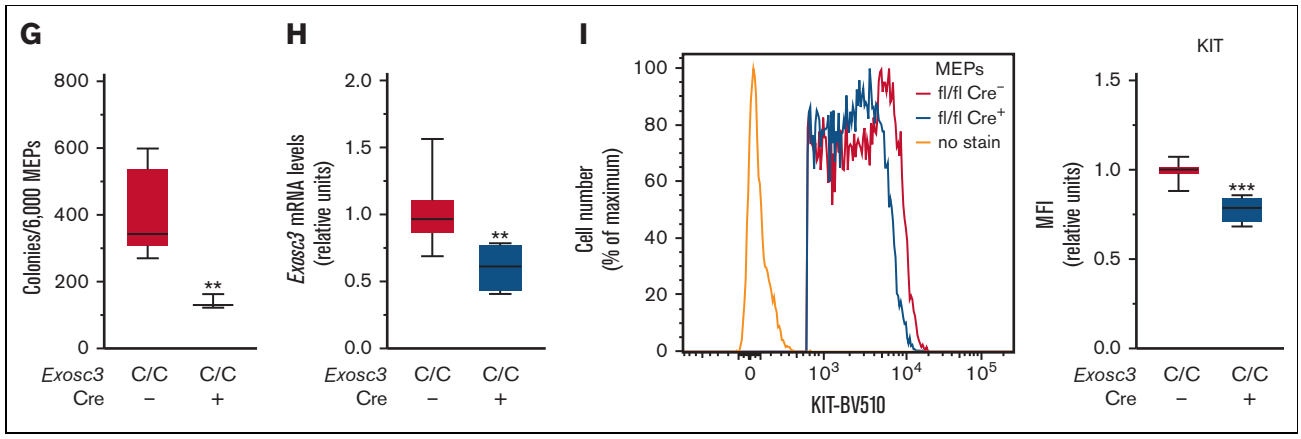

Figure 4 (continued) *Exosc3* ablation reduces MEP progenitor activity and immunophenotypic myeloid progenitors. (A) Experimental strategy. (B) Representative flow plot showing gating strategy. (C) Quantification of $Lin^-Sca\text{-}1^-KIT^+$ progenitors within Lin^- population. (D) Quantification of $KIT^+Fc\gamma R^-CD34^-$ MEPs, $KIT^+Fc\gamma R^-CD34^+$ CMPs, and $KIT^+Fc\gamma R^+CD34^+$ GMPs in *Exosc3*$^{C/C}$ Cre^- and *Exosc3*$^{C/C}$ Cre^+ fetal liver as a percentage of parent gate $Lin^-Sca\text{-}1^-KIT^+$ (LSK). (E) Total cell counts per E14.5 liver. (F) Quantification of MEP, CMP, and GMP cells per E14.5 fetal liver. (G) Colony quantitation from MEPs plated at 2000/mL (6 independent experiments: *Exosc3*$^{C/C}$ $Cre^- = 13$ and *Exosc3*$^{C/C}$ $Cre^+ = 3$). (H) quantitative reverse transcription PCR (qRT-PCR) quantitation of *Exosc3* mRNA from sorted MEPs. (I) KIT MFI quantitation in MEP population (7 independent experiments: *Exosc3*$^{C/C}$ $Cre^- = 17$ and *Exosc3*$^{C/C}$ $Cre^+ = 4$). Quantitative data are presented as box and whisker plots, with bounds from the 25th to 75th percentiles, the median line, and whiskers ranging from minimum to maximum values. $^*P < .05$, $^{**}P < .01$, and $^{***}P < .001$, by unpaired *t* test.

Exosc3$^{C/C}$ Cre^- fetal liver (11%) ($P < .0001$). CFU-E were reduced by 24% in *Exosc3*$^{C/C}$ Cre^+ (15.6%) fetal liver in comparison with *Exosc3*$^{C/C}$ Cre^- fetal liver (20.5%) ($P = .02$) (Figure 3C). With E14.5 fetal livers, 71% and 49% of BFU-E were GFP^+ with *Exosc3*$^{C/WT}$ Cre^+ and *Exosc3*$^{C/C}$ Cre^+ genotypes, respectively. GFP^+ progenitors were undetectable with control *Exosc3*$^{C/C}$ Cre^- fetal liver (Figure 3D).

Because the EC regulates KIT transcription and signaling in erythroid progenitors in vitro, we asked if this axis operates in vivo. *Exosc3*$^{C/C}$ Cre^+ embryos had 29% fewer KIT^+ Lin^- progenitors (70.9% and 54.3% with *Exosc3*$^{C/C}$ Cre^- and *Exosc3*$^{C/C}$ Cre^+ fetal livers, respectively ($P = .002$) (Figure 3E). In principle, this could reflect a decreased percentage of KIT-expressing cells, or fewer KIT molecules on the surface of KIT^+ cells, or both. In the Lin^- population, the KIT mean fluorescence intensity (MFI) was 48% lower in *Exosc3*$^{C/C}$ Cre^+ in comparison with *Exosc3*$^{C/C}$ Cre^- cells, reflected by loss of KIT-expressing cells and reduced intensity of fluorescence within the KIT^+ population ($P = .01$) (Figure 3F). In KIT^+ BFU-Es, the KIT MFI was 26% lower with *Exosc3*$^{C/C}$ Cre^+ in comparison with *Exosc3*$^{C/C}$ Cre^- ($P < .0001$) (Figure 3G). Because the EC processes 5.8S rRNA intermediate precursors,[1] we quantified these transcripts with sorted BFU-E. Primers were designed against the junction regions between ITS1 (internal transcribed spacer 1), 5.8S, and ITS2, and values were normalized to 18S, which had comparable expression between *Exosc3*$^{C/C}$ Cre^+ and *Exosc3*$^{C/C}$ Cre^- samples. In *Exosc3*$^{C/C}$ Cre^+ BFU-E, 5.8S-ITS2 transcripts increased 40% (from 1.21 to 1.48, $P = .01$), whereas ITS1-5.8S transcripts were unaffected ($P = .51$) (supplemental Figure 2A). Thus, *Exosc3* ablation during fetal development compromises immunophenotypic BFU-E, restricts KIT cell–surface expression, and elevates rRNA precursors in progenitors in vivo.

The committed erythroid BFU-E progenitor is derived from bipotent MEP, defined as $Lin^-Sca1^-KIT^+Fc\gamma R^-CD34^-$.[26-29] Because *Exosc3* ablation reduces immunophenotypic BFU-E and abrogates functional BFU-E, we asked if MEP levels and/or function were compromised. Within the Lin^- population, we quantified MEP, $Lin^-Sca1^-KIT^+Fc\gamma R^-CD34^+$ common myeloid progenitor (CMP), and $Lin^-Sca1^-KIT^+Fc\gamma R^+CD34^+$ granulocyte macrophage progenitor (GMP). E14.5 fetal livers were harvested, and MEPs were sorted from mutant and control embryos for RNA and CFU analyses (Figure 4A). In *Exosc3*$^{C/C}$ Cre^+ fetal liver, immunophenotypic MEPs increased in proportion relative to CMP and GMP, which were significantly reduced in comparison with control *Exosc3*$^{C/C}$ Cre^- fetal liver (Figure 4B). Although there was neither genotype-dependent difference in the $Lin^-Sca1^-KIT^+$ (55.6 ± 1.78 vs 51.3 ± 5, $P = .3$) nor in the $Lin^-Sca1^+KIT^+$ (LSK) populations (1.9 ± 0.4 vs 2.0 ± 1.1, $P = .8$) (Figure 4C; supplemental Figure 2B), MEPs increased by 10%, from 83% to 92% in comparison with control *Exosc3*$^{C/C}$ Cre^- fetal liver ($P < .0001$). CMPs and GMPs decreased twofold and threefold, respectively ($P = .01$ and $P = .0005$, respectively) (Figure 4D). Although the absolute number of fetal liver cells was unaltered (Figure 4E), the MEP cell number decreased by 1.6-fold ($P = .02$) in *Exosc3*$^{C/C}$ Cre^+ fetal liver, indicating that the increased percentage reflects the CMP and GMP loss in the $Lin^-Sca1^-KIT^+$ population, which decreased fourfold ($P = .005$) and sevenfold ($P = .002$), respectively, in absolute cell number in the *Exosc3*$^{C/C}$ Cre^+ fetal liver (Figure 4F). Despite the presence of immunophenotypic MEPs in *Exosc3*$^{C/C}$ Cre^+ fetal livers, these progenitors exhibited reduced CFU activity. MEP-derived colonies decreased by 66% from 403 ± 34 with *Exosc3*$^{C/C}$ Cre^- to 138 ± 12 with *Exosc3*$^{C/C}$ Cre^+ fetal liver ($P = .002$) (Figure 4G). *Exosc3* mRNA decreased by 40% in GFP^+ *Exosc3*$^{C/C}$ Cre^+–sorted MEPs ($P = .003$) (Figure 4H). Cell-surface KIT expression was 20% lower in *Exosc3*$^{C/C}$ Cre^+ MEPs ($P < .0001$) (Figure 4I). Although Exosc3 depletion affected progenitors upstream of BFU-E, the magnitude of alterations was less than that for

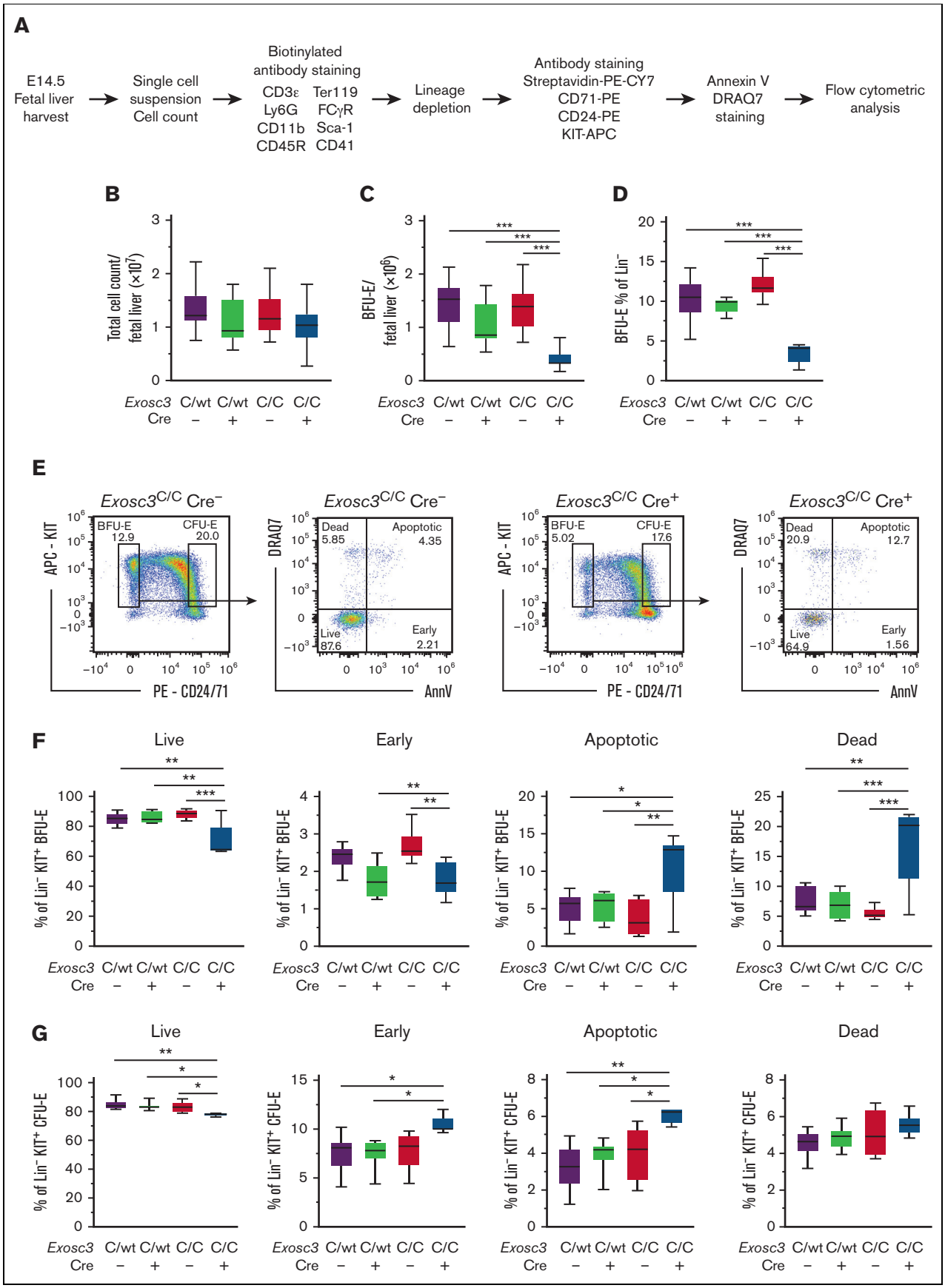
A
E14.5 Fetal liver harvest
Single cell suspension Cell count
Biotinylated antibody staining
CD3ε Ter119
Ly6G FCγR
CD11b Sca-1
CD45R CD41
Lineage depletion
Antibody staining
Streptavidin-PE-CY7
CD71-PE
CD24-PE
KIT-APC
Annexin V DRAQ7 staining
Flow cytometric analysis
B
Total cell count/ fetal liver (×10^7)
C
BFU-E/ fetal liver (×10^6)
D
BFU-E % of Lin−
Exosc3 C/wt C/wt C/C C/C
Cre − + − +
E
Exosc3C/C Cre−
Exosc3C/C Cre+
APC - KIT
PE - CD24/71
DRAQ7
AnnV
BFU-E 12.9
CFU-E 20.0
Dead 5.85
Apoptotic 4.35
Live 87.6
Early 2.21
BFU-E 5.02
CFU-E 17.6
Dead 20.9
Apoptotic 12.7
Live 64.9
Early 1.56
F
Live
Early
Apoptotic
Dead
% of Lin− KIT+ BFU-E
G
% of Lin− KIT+ CFU-E

Figure 5.

erythroid-committed progenitors, which were exceptionally sensitive to *Exosc3* ablation.

Exosc3 ensures early erythroid progenitor survival in vivo

We asked if *Exosc3* ablation in vivo affects erythroid progenitor viability. Erythroid progenitors were isolated, stained with annexin V and DRAQ7, and analyzed by flow cytometry (Figure 5A). With E14.5 fetal liver and comparable total cell counts (Figure 5B), the absolute number of $Lin^{-}KIT^{+}CD24/71^{10\%low}$ BFU-E decreased significantly from 1.3×10^6 to 0.4×10^6 with $Exosc3^{C/C}$ Cre^{-} and $Exosc3^{C/C}$ Cre^{+} conditions, respectively ($P < .0001$) (Figure 5C). As a percentage of Lin^{-} progenitors, $Lin^{-}KIT^{+}CD24/71^{10\%low}$ BFU-E decreased 61% from 11% to 4.3% with $Exosc3^{C/C}$ Cre^{-} and $Exosc3^{C/C}$ Cre^{+} conditions, respectively, ($P < .0001$) (Figure 5D).

Within the BFU-E population, apoptotic cells ($AnnV^{+}DRAQ7^{+}$) increased threefold from 3.7 ± 1.0 to 11 ± 1.9 with $Exosc3^{C/C}$ Cre^{-} and $Exosc3^{C/C}$ Cre^{+} conditions, respectively ($P = .003$). Dead cells ($AnnV^{-}DRAQ7^{+}$) increased by 3.1-fold from 5.4 ± 0.4 to 17 ± 2.7 with $Exosc3^{C/C}$ Cre^{-} and $Exosc3^{C/C}$ Cre^{+} conditions, respectively, ($P = .0002$) (Figure 5E-F). Live cells ($AnnV^{-}DRAQ7^{-}$) decreased by 20% from 88 ± 1.3 to 70 ± 4.4 ($P = .0006$) and early apoptotic cells ($AnnV^{+}DRAQ7^{-}$) decreased by 33% from 2.7 ± 0.1 to 1.8 ± 0.1 ($P = .009$) (Figure 5F). With CFU-E, there was a 6.1% decrease in live cells from 83 ± 1.5 to 78 ± 0.3 ($P = .03$) and 1.5-fold increase in apoptotic cells (4.0 ± 0.5-6.1 ± 0.1 with $Exosc3^{C/C}$ Cre^{-} and $Exosc3^{C/C}$ Cre^{+}, respectively, $P = .01$), with no change in early apoptotic or dead cells, in comparison with the $Exosc3^{C/C}$ Cre^{-} condition (Figure 5G). Thus, the EC is a determinant of erythroid progenitor survival in vivo, with BFU-E exhibiting the greatest sensitivity to *Exosc3* ablation.

To elucidate the mechanism by which the EC confers erythroid progenitor survival, RNA-seq was conducted to ask how *Exosc3* ablation affects the BFU-E transcriptome. GFP^{+} $Lin^{-}KIT^{+}CD24/71^{10\%low}$ BFU-E and GFP^{-} $Lin^{-}KIT^{+}CD24/71^{10\%low}$ BFU-E were sorted from $Exosc3^{C/C}Cre^{+}$ embryos and $Exosc3^{C/C}$ Cre^{-} embryos, respectively, for CFU and RNA-seq analyses (Figure 6A-B; supplemental Figure 2C). DAPI staining was used to assess cell viability, and $DAPI^{-}$ cells were sorted for subsequent analyses (Figure 6C). Immunophenotypic BFU-E were twofold lower in the Lin^{-} population (Figure 6D). Sorted BFU-E were also analyzed in the CFU assay, and *Exosc3*-ablated progenitors did not form colonies (Figure 6E).

The RNA-seq analysis quantified 48 893 annotated genes, and 11 422 genes had, within at least 1 genotype group, mean FPKM >1 and nonzero abundance in all samples of that group (Figure 6F). Among these genes, 530 were differentially expressed genes with an adjusted $P < .05$ with $Exosc3^{C/C}$ Cre^{+} BFU-E in comparison with control $Exosc3^{C/C}$ Cre^{-} BFU-E. A total of 276 and 254 of the differentially expressed genes were downregulated and upregulated, respectively (Figure 6G). GFP transcripts were only detected in $Exosc3^{C/C}$ Cre^{+} samples, and all replicates had comparable gene expression distribution and average number of reads, and biological replicates were segregated by principal component analysis (supplemental Figure 2D-G)

GO analysis of downregulated genes yielded 110 categories, including basic cellular processes and immune response (not shown). Because transcript upregulation is likely to be a direct consequence of reduced EC activity, we further analyzed the upregulated transcripts. The GO analysis for upregulated genes revealed a restricted cohort of categories (Figure 6H), including components of the p53-mediated apoptosis pathway, which increased significantly in *Exosc3*-ablated BFU-Es. The p53 target genes *Mdm2*, *Trp53inp1*, *Cdkn1a*, and *Phlda3* were upregulated significantly in $Exosc3^{C/C}$ Cre^{+} BFU-Es. We mined transcriptome and proteome data, which revealed *Trp53inp1*, *Mdm2*, and *Cdkn1a* transcripts to be GATA1-induced in the G1E-ER-GATA1 genetic complementation system.[15,30] The quantitative proteomic analysis, which sampled a subset of cellular proteins, identified Trp53inp1 as being GATA1-induced (4.9-fold) (supplemental Figure 3A-B). GATA2 upregulated *Mdm2* and *Pmaip1* and decreased *Mybbp1a* transcripts in GATA2-deficient myeloid progenitors lacking the *Gata2*-77 enhancer[28,31] (supplemental Figure 3C).

We deployed a prioritization strategy based on fold change, transcript abundance, whether the gene was expressed in the erythroid lineage, and whether the gene was known to regulate cell survival/death. This analysis yielded 14 genes that were subjected to validation by qRT-PCR. *Exosc3* mRNA was 50% lower in GFP^{+} BFU-E from $Exosc3^{C/C}Cre^{+}$ fetal livers. Comparison of GFP^{+} BFU-E from $Exosc3^{C/C}Cre^{+}$ fetal livers and GFP^{-} BFU-E from $Exosc3^{C/C}Cre^{-}$ fetal livers revealed that the levels of diverse transcripts important for erythroid biology, such as, *Kit*, *Epor*, *Gata1*, and globin genes, were unaltered (supplemental Table 1; supplemental Figures 3D and 4B). *Exosc3* ablation increased accumulation of *Bax*, *Bbc3/Puma*, and *Pmaip1/Noxa* transcripts, encoding members of the BCL-2 protein family of proapoptotic factors that function in the intrinsic apoptosis pathway. *Bax* transcripts increased 2.3-fold ($P = .0001$), *Bbc3* increased fivefold ($P < .0001$), and *Pmaip1* increased fourfold ($P = .003$), with $Exosc3^{C/C}$ Cre^{+} in comparison with $Exosc3^{C/C}$ Cre^{-} BFU-E (supplemental Figure 4A-B). In addition to upregulation of intrinsic apoptotic pathway components, *Exosc3* ablation increased *Fas* (*Tnfrsf6*, tumor necrosis factor receptor superfamily 6) transcripts, which encode the death receptor Fas. *Fas* mRNA increased 23-fold, whereas *FasL,* encoding its ligand, was undetectable in the analysis (supplemental Figure 4A). The integral membrane proteins Fas and FasL are members of the tumor necrosis factor receptor superfamily. The transcriptomic landscape of *Exosc3*-ablated BFU-E, isolated by flow cytometry to ensure cell viability, revealed the upregulation of multiple cohorts of proapoptotic

Figure 5. *Exosc3* ablation compromises erythroid progenitor survival. (A) Experimental strategy. (B) Fetal liver live cell counts. Dead cells were excluded by trypan blue. (C) KIT^{+} BFU-E cell counts per E14.5 fetal liver. (D) BFU-E as percentage of lineage-depleted precursors (4 independent experiments: n = 33). (E) Representative flow cytometric plots for control $Exosc3^{C/C}$ Cre^{-} and $Exosc3^{C/C}$ Cre^{+}. (F) Percentage of BFU-E in live ($AnnV^{-}DRAQ7^{-}$), early apoptotic ($AnnV^{+}DRAQ7^{-}$), late apoptotic ($AnnV^{+}DRAQ7^{+}$), and dead ($AnnV^{-}DRAQ7+$) cells, based on annexin V and DRAQ7 staining. Quantitative data are presented as box and whisker plots, with bounds from the 25th to 75th percentiles, the median line, and whiskers ranging from minimum to maximum values. $^{*}P < .05$, $^{**}P < .01$, and $^{***}P < .001$, by Tukey multiple comparisons test. (G) Percentage of CFU-E in live, early apoptotic, late apoptotic, and dead cells (3 independent experiments: $Exosc3^{C/C}$ Cre^{-} = 6, $Exosc3^{C/WT}$ Cre^{-} =6, $Exosc3^{C/WT}$ Cre^{+} = 6, and $Exosc3^{C/C}$ Cre^{+} = 6).

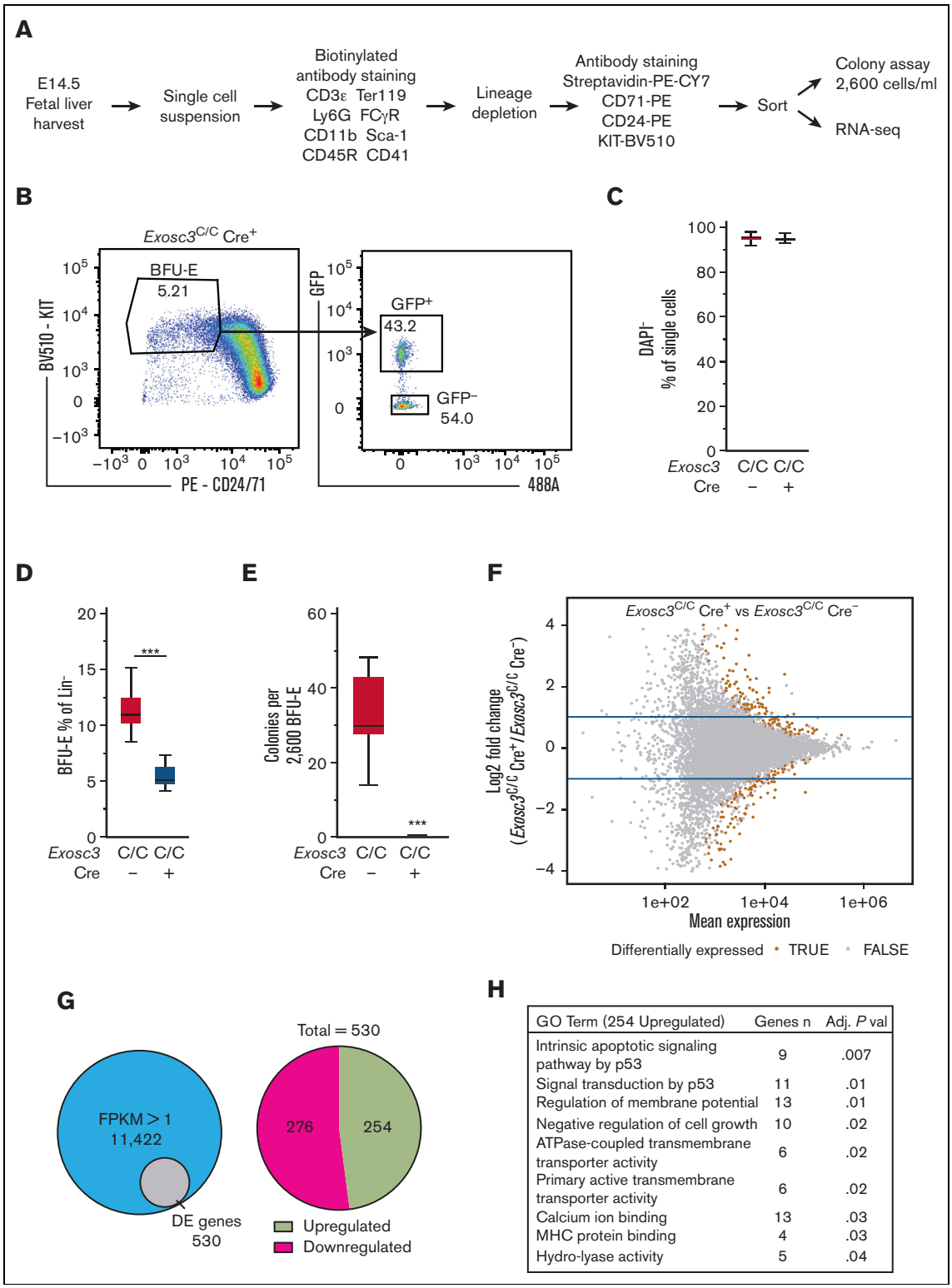

GO Term (254 Upregulated)	Genes n	Adj. *P* val
Intrinsic apoptotic signaling pathway by p53	9	.007
Signal transduction by p53	11	.01
Regulation of membrane potential	13	.01
Negative regulation of cell growth	10	.02
ATPase-coupled transmembrane transporter activity	6	.02
Primary active transmembrane transporter activity	6	.02
Calcium ion binding	13	.03
MHC protein binding	4	.03
Hydro-lyase activity	5	.04

Figure 6. Exosc3 downregulates transcripts encoding proapoptotic factors. (A) Experimental strategy. (B) Representative flow cytometric plot of sorted GFP$^+$ BFU-E from *Exosc3*$^{C/C}$ Cre$^+$ fetal liver (3 independent experiments: *Exosc3*$^{C/C}$ Cre$^-$ = 3 and *Exosc3*$^{C/C}$ Cre$^+$ = 3). (C) DAPI staining was used to exclude dead cells. (D) Quantification of Lin$^-$ KIT$^+$ BFU-E in *Exosc3*$^{C/C}$ Cre$^-$ and *Exosc3*$^{C/C}$ Cre$^+$ fetal liver sorted for RNA-seq analysis. (E) BFU-E quantification from the same biological replicates analyzed by RNA-seq. Cells were plated at 2600/mL (6 independent experiments: *Exosc3*$^{C/C}$ Cre$^-$ = 12 and *Exosc3*$^{C/C}$ Cre$^+$ = 7). Quantitative data are presented as box and whisker plots, with bounds from the 25th to 75th percentiles, the median line, and whiskers ranging from minimum to maximum values. *$P < .05$, **$P < .01$, and ***$P < .001$, by unpaired *t* test. (F) MA plot resulting from differential expression analysis between *Exosc3*$^{C/C}$ Cre$^-$ and *Exosc3*$^{C/C}$ Cre$^+$ BFU-E. The brown circles depict significant differentially expressed (DE) transcripts. (G) The Venn diagram illustrates 530 DE genes out of 11 422 genes detected with fragments per kilobase of transcripts per million mapped reads (FPKM) >1 (left).

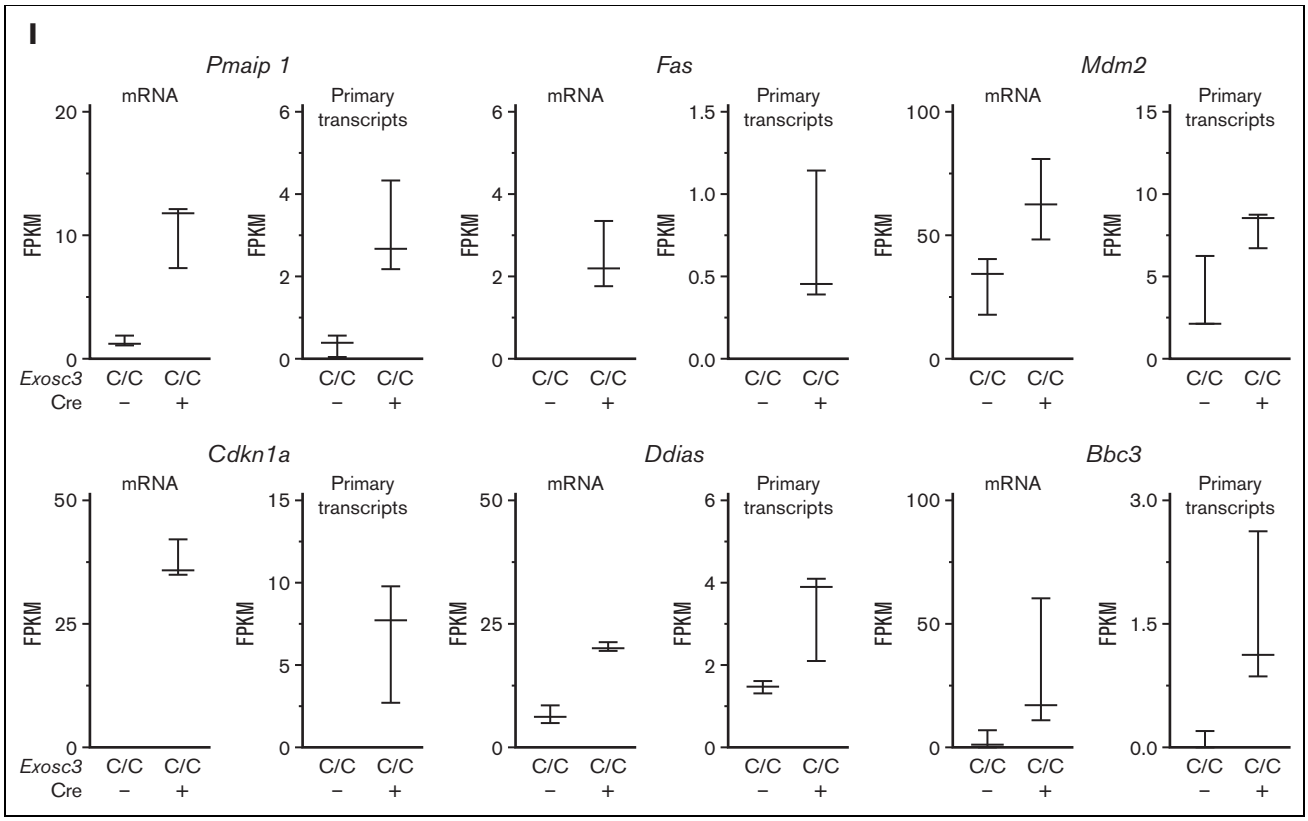

Figure 6 (continued) 530 DE genes were parsed into 254 upregulated and 276 downregulated transcripts (right). (H) Gene ontology (GO) analysis with 254 upregulated genes revealed apoptosis-related categories as top hits. (I) FPKM values for mRNA and primary transcripts of apoptosis-regulatory genes from prioritized list with highest fold change between *Exosc3*$^{C/C}$ Cre^{+} and *Exosc3*$^{C/C}$ Cre^{-} BFU-E. DE, differentially expressed.

genes. Quantitative analysis of mRNA and primary transcripts from the RNA-seq data revealed that *Exosc3* ablation elevated mRNAs and primary transcripts (Figure 6I; supplemental Figure 5), consistent with a model in which the EC suppresses a proapoptotic transcriptional program in erythroid progenitor cells.

Discussion

Because the EC regulates diverse RNA species, one would predict that it is broadly important in all cell types. The hematopoietic system, in which stem and progenitor cells are generated and function at distinct anatomical sites during embryogenesis, constitutes an attractive model to address whether the EC is critical in all or a circumscribed cohort of cell types. An important component of hematopoiesis requires population of the fetal liver with aorta-gonad-mesonephros–generated HSCs.[32] The fetal liver also harbors abundant progenitors generated from erythrocyte macrophage progenitors (EMPs) that arise in the yolk sac.[33-35] Given our in vitro studies demonstrating that EC disruption is deleterious to erythroid progenitors,[6,16,17] we used a *Vav1*-Cre system to evaluate EC function in the hematopoietic system in vivo, with an emphasis on erythrocyte development. *Vav1*-Cre–mediated *Exosc3* ablation reduced, but did not eliminate, *Exosc3* expression from hematopoietic progenitors owing to monoallelic recombination and/or cells resistant to ablation. Despite this reduced *Exosc3* expression, *Exosc3*-ablated E12.5 and 14.5 embryos were morphologically normal, with a small reduction in fetal liver cellularity. However, the fetal livers were devoid of functional erythroid progenitors, and embryonic lethality occurred after E14.5.

Exosc3-ablated fetal liver contained large numbers of GFP^{-} progenitors harboring a WT locus and normal *Exosc3* mRNA levels, consistent with a lack of *Vav1*-Cre action in these cells and their precursors. Although *Vav1*-Cre is used commonly to generate hematopoietic-specific knockouts,[20,22,23,36] whether *Vav1* is invariably inactive or active in yolk sac–derived progenitors in different systems is unresolved. GATA1 represses *Exosc3* transcription,[6,17] and once GFP is expressed from a recombined locus, the locus is predicted to retain GATA1 responsiveness. GATA1 repression of the recombined locus will generate cells lacking GFP transcripts, and some dividing cells might become GFP^{-}. However, structural analysis revealed recombination exclusively with sorted GFP^{+}, but not GFP^{-}, erythroid progenitors. GFP^{-} progenitors expressed *Exosc3* mRNA at levels comparable to control progenitors. GFP^{-} cells may arise from yolk sac–derived progenitors that do not express *Vav1*, for example, EMPs that generate erythroid and myeloid cells to sustain embryogenesis or the selective expansion of residual WT cells. Assessing EC function in EMPs will require alternative strategies, and critical EC functions in other sectors of the hematopoietic system cannot be ruled out, as transplantation analyses are required. It will be instructive to use other conditional knockout systems to analyze lineage-specific EC

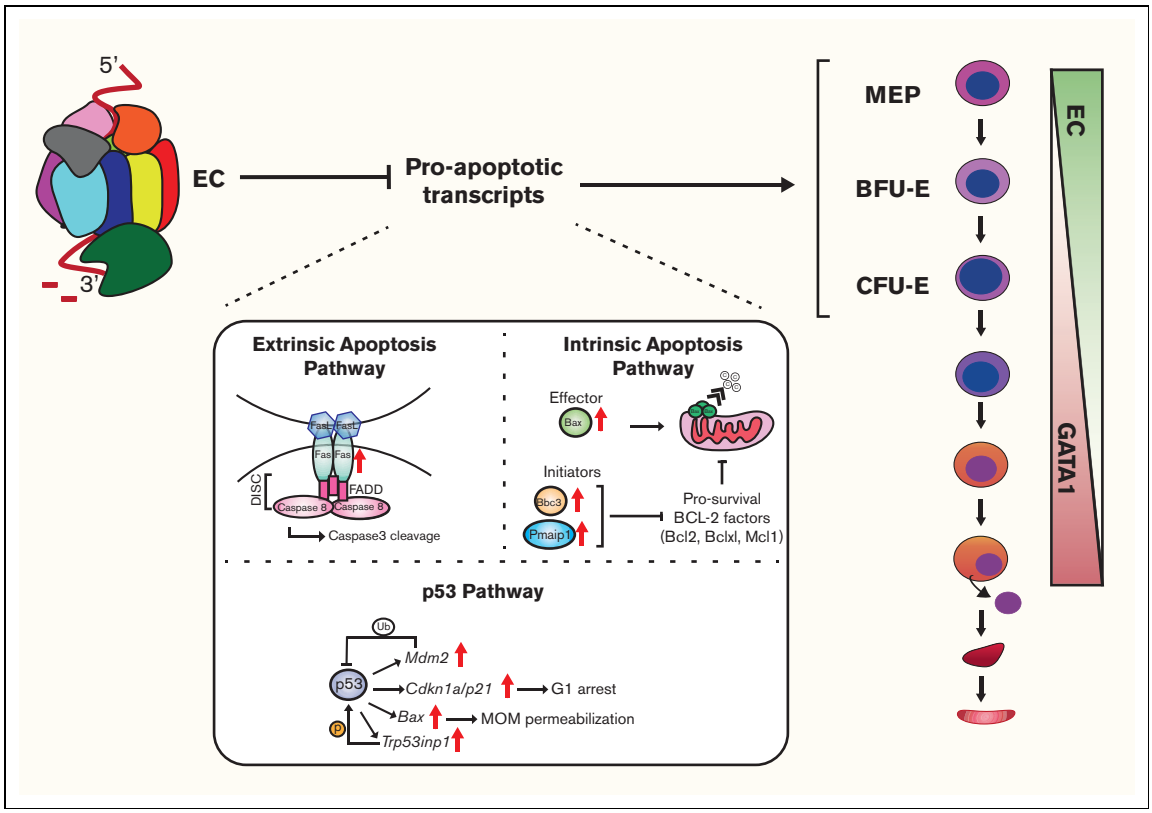

Figure 7. EC confers erythroid progenitor survival and function in vivo. *Vav1*-Cre–mediated *Exosc3* ablation in the hematopoietic system is embryonically lethal after E14.5. *Exosc3* expression is required for erythroid and myeloid progenitor activity. In *Exosc3*-ablated embryos, immunophenotypic BFU-Es are reduced, and progenitor activity is abrogated. MEPs can still be detected but have reduced activity. RNA-seq analysis of sorted GFP$^+$ BFU-E revealed accumulation of proapoptotic genes, and *Exosc3*-ablated progenitors became apoptotic. During erythroid maturation, GATA1 represses genes encoding EC subunits.[6,16,17] Before repression, the EC establishes and/or maintains functional erythroid progenitors, which involves conferring KIT expression/signaling, protection against DNA damage,[6] and suppressing, directly or indirectly, a proapoptotic program.

functions during adult hematopoiesis. Our results demonstrate a hematopoietic cell–intrinsic requirement of an essential EC subunit for erythroid progenitor activity.

The nearly complete lack of erythroid progenitor activity was not accompanied by a quantitative depletion of immunophenotypic erythroid progenitors. *Exosc3* ablation decreased immunophenotypic BFU-E by ~50%. As the erythroid progenitor CFU assay involves an 8-day culture and *Exosc3* ablation elevates transcripts encoding proapoptotic factors, progenitor viability may decrease as a function of time after progenitor culture. As immunophenotypic erythroid progenitors were not quantitatively eliminated, *Exosc3* ablation did not eliminate the capacity of MEPs to generate BFU-E or at least functionally defective cells with BFU-E attributes.

Transcripts encoding proapoptotic factors, including intrinsic apoptotic pathway components Bbc3, Bax, and Pmaip1, were upregulated in *Exosc3*-ablated BFU-E. The BCL-2 family contains the BH3 (BCL-2 homology 3)–only members (*Bbc3*, *Bad*, *Bid*, *Bik*, *Bim*, *Noxa*, *Bmf*, and *Hrk*), prosurvival factors (*Bcl2*, *Mcl-1*, *Bcl2l1*, *Bcl2l2*, and *Bcl2a1*), and proapoptotic factors (*Bax*, *Bak*, and *Bok*)[37] (supplemental Table 2). Conditional BCL-XL ablation induces anemia due to a BCL-XL requirement in reticulocytes. Loss of the BH3-only domain factors, BIM and PUMA, does not rescue the phenotype, indicating that these proapoptotic factors do not mediate apoptosis without BCL-XL during adult erythropoiesis.[38] PUMA and NOXA function during embryonic erythropoiesis have not been fully characterized. The antiapoptotic protein MCL-1 confers erythroid progenitor survival before BCL-XL expression at later stages. BAX is highly expressed in a population enriched for proerythroblasts (CD71$^+$ Ter119$^-$) and early basophilic erythroblasts (CD71$^+$ Ter119^{low}).[39] Although *Mcl1* and *Bcl2l1* (encoding BCL-XL) transcripts detected by our RNA-seq analysis were not significantly different between *Exosc3*$^{C/C}$ Cre$^+$ and Exosc3$^{C/C}$ Cre$^-$ conditions, qRT-PCR analysis revealed a 1.3-fold increase (P = .004) in *Bcl2l1* transcripts. Primary transcripts and mRNA encoding the death receptor, FAS, were also detected at increased levels in mutant embryos. In splenic stress erythropoiesis, the interaction between Fas and FasL regulates apoptosis, which is suppressed by prosurvival EPO signaling.[40] During fetal liver development, Fas and FasL negatively regulate erythroid progenitor expansion, limiting mature cell generation.[41] Mechanistically, primary transcript upregulation suggests an EC-suppressed transcriptional mechanism, as the EC directly and indirectly controls genome function[3,42,43] or EC-dependent destruction of primary transcripts.[44]

Considering that Exosc3 confers erythroid progenitor function, survival, and suppresses apoptosis-regulatory transcripts, we propose that the EC limits the levels of proapoptotic factors in erythroid progenitors (Figure 7), and once GATA1 represses EC genes, distinct mechanisms are deployed to balance pro- and antiapoptotic factors. Further studies are required to establish if EC directly controls the levels of apoptotic transcripts, as EC subunit downregulation disrupts RNA processing and induces DNA damage and apoptosis.[5,6] The GATA1/EC axis confers maximal stem cell factor signaling in erythroid progenitors ex vivo,[17] and stem cell factor signaling supports survival and proliferation.[45] *Kit* and *Epor* transcript levels were unaltered in *Exosc3*-ablated erythroid progenitors, which might reflect the partial loss of *Exosc3* and/or subunit-specific requirements for the control of cellular signaling. It will be instructive to consider whether this EC-apoptosis link can be extrapolated to other sectors of the hematopoietic system and nonhematopoietic contexts in which the EC may also exert vital functions in stem and/or progenitor cells. Analogous to the GATA1-regulated network of genes and proteins that inform mechanisms of erythropoiesis and, more broadly, cellular differentiation, the EC-dependent transcriptome established herein, which supports progenitor cells, will almost certainly unveil new paradigms.

Acknowledgments

The authors thank the University of Wisconsin Biotechnology Center DNA Sequencing Facility and the Carbone Cancer Center Flow Cytometry Laboratory for providing sequencing and flow cytometry services, respectively.

This work was supported by grants from the National Institute of Diabetes and Digestive and Kidney Diseases (NIHDK50107) (E.H.B.), National Institute of Allergy and Infectious Diseases (NIHAI143897) (U.B.), and Carbone Cancer Center (P30CA014520). I.F.d.A. was supported in part by funding from Coordenação de Aperfeiçoamento de Pessoal de Nível Superior (CAPES), Brazil.

Authorship

Contribution: I.F.d.A. performed experiments and constructed the figures and graphs; I.F.d.A. and K.D.J. analyzed results; C.N.D. conducted RNA sequencing analysis; U.B. provided *Exosc3*-floxed animals and primers; and I.F.d.A., C.M., and E.H.B. designed the research and wrote the manuscript.

Conflict-of-interest disclosure: The authors declare no competing financial interests.

ORCID profiles: I.F.d.A., 0000-0001-5997-094X; C.M., 0000-0002-8644-3333; C.N.D., 0000-0003-1498-9254; E.H.B., 0000-0002-1151-5654.

Correspondence: Emery H. Bresnick, Department of Cell and Regenerative Biology, Carbone Cancer Center, University of Wisconsin School of Medicine and Public Health, 1111 Highland Ave, 4009 WIMR, Madison, WI 53705; email: ehbresni@wisc.edu.

References

1. Mitchell P, Petfalski E, Shevchenko A, Mann M, Tollervey D. The exosome: a conserved eukaryotic RNA processing complex containing multiple 3'–>5' exoribonucleases. *Cell*. 1997;91(4):457-466.
2. Schuller JM, Falk S, Fromm L, Hurt E, Conti E. Structure of the nuclear exosome captured on a maturing preribosome. *Science*. 2018;360(6385):219-222.
3. Pefanis E, Wang J, Rothschild G, et al. RNA exosome-regulated long non-coding RNA transcription controls super-enhancer activity. *Cell*. 2015;161(4):774-789.
4. Pefanis E, Wang J, Rothschild G, et al. Noncoding RNA transcription targets AID to divergently transcribed loci in B cells. *Nature*. 2014;514(7522):389-393.
5. Fraga de Andrade I, Mehta C, Bresnick EH. Post-transcriptional control of cellular differentiation by the RNA exosome complex. *Nucleic Acids Res*. 2020;48(21):11913-11928.
6. Mehta C, Fraga de Andrade I, Matson DR, Dewey CN, Bresnick EH. RNA-regulatory exosome complex confers cellular survival to promote erythropoiesis. *Nucleic Acids Res*. 2021;49(16):9007-9025.
7. Meola N, Domanski M, Karadoulama E, et al. Identification of a nuclear exosome decay pathway for processed transcripts. *Mol Cell*. 2016;64(3):520-533.
8. Wu M, Karadoulama E, Lloret-Llinares M, et al. The RNA exosome shapes the expression of key protein-coding genes. *Nucleic Acids Res*. 2020;48(15):8509-8528.
9. Tsai SF, Martin DI, Zon LI, D'Andrea AD, Wong GG, Orkin SH. Cloning of cDNA for the major DNA-binding protein of the erythroid lineage through expression in mammalian cells. *Nature*. 1989;339(6224):446-451.
10. Evans T, Felsenfeld G. The erythroid-specific transcription factor Eryf1: a new finger protein. *Cell*. 1989;58(5):877-885.
11. Welch JJ, Watts JA, Vakoc CR, et al. Global regulation of erythroid gene expression by transcription factor GATA-1. *Blood*. 2004;104(10):3136-3147.
12. Fujiwara T, O'Geen H, Keles S, et al. Discovering hematopoietic mechanisms through genome-wide analysis of GATA factor chromatin occupancy. *Mol Cell*. 2009;36(4):667-681.
13. Yu M, Riva L, Xie H, et al. Insights into GATA-1-mediated gene activation versus repression via genome-wide chromatin occupancy analysis. *Mol Cell*. 2009;36(4):682-695.

14. Cheng Y, Wu W, Kumar SA, et al. Erythroid GATA1 function revealed by genome-wide analysis of transcription factor occupancy, histone modifications, and mRNA expression. *Genome Res*. 2009;19(12):2172-2184.
15. Tanimura N, Miller E, Igarashi K, et al. Mechanism governing heme synthesis reveals a GATA factor/heme circuit that controls differentiation. *EMBO Rep*. 2016;17(2):249-265.
16. McIver SC, Kang YA, DeVilbiss AW, et al. The exosome complex establishes a barricade to erythroid maturation. *Blood*. 2014;124(14):2285-2297.
17. McIver SC, Katsumura KR, Davids E, et al. Exosome complex orchestrates developmental signaling to balance proliferation and differentiation during erythropoiesis. *Elife*. 2016;5:e17877.
18. Oddone A, Lorentzen E, Basquin J, et al. Structural and biochemical characterization of the yeast exosome component Rrp40. *EMBO Rep*. 2007;8(1):63-69.
19. Weick EM, Puno MR, Januszyk K, Zinder JC, DiMattia MA, Lima CD. Helicase-dependent RNA decay illuminated by a Cryo-EM structure of a human nuclear RNA exosome-MTR4 complex. *Cell*. 2018;173(7):1663-1677.e21.
20. Ogilvy S, Metcalf D, Gibson L, Bath ML, Harris AW, Adams JM. Promoter elements of vav drive transgene expression in vivo throughout the hematopoietic compartment. *Blood*. 1999;94(6):1855-1863.
21. de Boer J, Williams A, Skavdis G, et al. Transgenic mice with hematopoietic and lymphoid specific expression of Cre. *Eur J Immunol*. 2003;33(2):314-325.
22. Stadtfeld M, Graf T. Assessing the role of hematopoietic plasticity for endothelial and hepatocyte development by non-invasive lineage tracing. *Development*. 2005;132(1):203-213.
23. Chen MJ, Yokomizo T, Zeigler BM, Dzierzak E, Speck NA. Runx1 is required for the endothelial to haematopoietic cell transition but not thereafter. *Nature*. 2009;457(7231):887-891.
24. Damnernsawad A, Kong G, Wen Z, et al. Kras is required for adult hematopoiesis. *Stem Cells*. 2016;34(7):1859-1871.
25. Li H, Natarajan A, Ezike J, et al. Rate of progression through a continuum of transit-amplifying progenitor cell states regulates blood cell production. *Dev Cell*. 2019;49(1):118-129.e7.
26. Akashi K, Traver D, Miyamoto T, Weissman IL. A clonogenic common myeloid progenitor that gives rise to all myeloid lineages. *Nature*. 2000;404(6774):193-197.
27. Traver D, Miyamoto T, Christensen J, Iwasaki-Arai J, Akashi K, Weissman IL. Fetal liver myelopoiesis occurs through distinct, prospectively isolatable progenitor subsets. *Blood*. 2001;98(3):627-635.
28. Johnson KD, Kong G, Gao X, et al. Cis-regulatory mechanisms governing stem and progenitor cell transitions. *Sci Adv*. 2015;1(8):e1500503.
29. Mehta C, Johnson KD, Gao X, et al. Integrating enhancer mechanisms to establish a hierarchical blood development program. *Cell Rep*. 2017;20(12):2966-2979.
30. Tanimura N, Liao R, Wilson GM, et al. GATA/heme multi-omics reveals a trace metal-dependent cellular differentiation mechanism. *Dev Cell*. 2018;46(5):581-594.e4.
31. Johnson KD, Conn DJ, Shishkova E, et al. Constructing and deconstructing GATA2-regulated cell fate programs to establish developmental trajectories. *J Exp Med*. 2020;217(11):e20191526.
32. Dzierzak E, Speck NA. Of lineage and legacy: the development of mammalian hematopoietic stem cells. *Nat Immunol*. 2008;9(2):129-136.
33. Soares-da-Silva F, Freyer L, Elsaid R, et al. Yolk sac, but not hematopoietic stem cell-derived progenitors, sustain erythropoiesis throughout murine embryonic life. *J Exp Med*. 2021;218(4):e20201729.
34. McGrath KE, Frame JM, Fegan KH, et al. Distinct sources of hematopoietic progenitors emerge before HSCs and provide functional blood cells in the mammalian embryo. *Cell Rep*. 2015;11(12):1892-1904.
35. Schulz C, Gomez Perdiguero E, Chorro L, et al. A lineage of myeloid cells independent of Myb and hematopoietic stem cells. *Science*. 2012;336(6077):86-90.
36. Ghiaur G, Ferkowicz MJ, Milsom MD, et al. Rac1 is essential for intraembryonic hematopoiesis and for the initial seeding of fetal liver with definitive hematopoietic progenitor cells. *Blood*. 2008;111(7):3313-3321.
37. Czabotar PE, Lessene G, Strasser A, Adams JM. Control of apoptosis by the BCL-2 protein family: implications for physiology and therapy. *Nat Rev Mol Cell Biol*. 2014;15(1):49-63.
38. Delbridge AR, Aubrey BJ, Hyland C, et al. The BH3-only proteins BIM and PUMA are not critical for the reticulocyte apoptosis caused by loss of the pro-survival protein BCL-XL. *Cell Death Dis*. 2017;8(7):e2914.
39. Turnis ME, Kaminska E, Smith KH, et al. Requirement for antiapoptotic MCL-1 during early erythropoiesis. *Blood*. 2021;137(14):1945-1958.
40. Liu Y, Pop R, Sadegh C, Brugnara C, Haase VH, Socolovsky M. Suppression of Fas-FasL coexpression by erythropoietin mediates erythroblast expansion during the erythropoietic stress response in vivo. *Blood*. 2006;108(1):123-133.
41. Socolovsky M, Murrell M, Liu Y, Pop R, Porpiglia E, Levchenko A. Negative autoregulation by FAS mediates robust fetal erythropoiesis. *PLoS Biol*. 2007;5(10):e252.
42. Camblong J, Iglesias N, Fickentscher C, Dieppois G, Stutz F. Antisense RNA stabilization induces transcriptional gene silencing via histone deacetylation in S. cerevisiae. *Cell*. 2007;131(4):706-717.

43. Lim SJ, Boyle PJ, Chinen M, Dale RK, Lei EP. Genome-wide localization of exosome components to active promoters and chromatin insulators in Drosophila. *Nucleic Acids Res*. 2013;41(5):2963-2980.

44. Lubas M, Andersen PR, Schein A, Dziembowski A, Kudla G, Jensen TH. The human nuclear exosome targeting complex is loaded onto newly synthesized RNA to direct early ribonucleolysis. *Cell Rep*. 2015;10(2):178-192.

45. Kurata H, Mancini GC, Alespeiti G, Migliaccio AR, Migliaccio G. Stem cell factor induces proliferation and differentiation of fetal progenitor cells in the mouse. *Br J Haematol*. 1998;101(4):676-687.